Università degli Studi di Padova
Dipartimento di Ingegneria Industriale

Corso di Laurea in
Fisica

FULL-WAVE ANALYSIS OF NONUNIFORM HELICON PLASMA SOURCES FOR ELECTRIC PROPULSION SYSTEMS

Relatore

Ch.mo Prof. Daniele Pavarin

Correlatore

Ch.mo Dott. Davide Melazzi

Laureando: Lorenzo Berto

Matricola: 1005060

Anno Accademico 2013 - 2014

Dedicated to my parents

Contents

Abstract

A Helicon plasma source is a high-density, high-efficiency plasma source that sustains steady plasma production through the absorption and propagation of helicon waves. A typical Helicon plasma source is comprised of: (i) a gas feeding system; (ii) a cylindrically-shaped plasma column; (iii) magnetic coils for plasma confinement; (iv) an RF antenna working at MHz frequencies. Helicon plasma sources have been employed in many industrial processes and lately also in space propulsion. The propulsive figures of merit of an HPT (e.g., thrust efficiency, specific impulse) depend on the power deposited by the antenna into the plasma, which is related to the real part of the antenna impedance.
In this work we have investigated the power deposition of three different RF antennas (i.e., the Single-Loop, the Nagoya Type-III and the Fractional Helix) into a non-uniform plasma with parabolic profile along the radial direction and Gaussian profile along the axial direction, as a function of plasma discharge parameters (e.g., bulk and edge plasma densities, electron temperature, neutral background pressure).
We have relied on ADAMANT, a full-wave numerical tool based on a set of coupled surface and volume integral equations. The explored ranges of plasma discharge parameters are: (i) magneto-static field below < 1000 G; (ii) bulk plasma density from 10^{18} m^{-3} to 10^{19} m^{-3}, edge plasma density from 10^{17} m^{-3} to 5×10^{18} m^{-3}; (iii) electron temperature from 3 eV to 7 eV; (iv) neutral background pressure from 15 mTorr to 30 mTorr.
Results show that plasma density profiles only affect the magnitude of the real part of the impedance, while the trend of the power deposition curves as functions of the magneto-static field values is influenced by the bulk plasma density value. Radial and radial-axial density profiles have similar trends in power deposition for all the antennas and plasma discharge parameters considered. The amount of power coupled into the plasma also depends on the magneto-static field value and the antenna geometry, while the electron temperature and the neutral background pressure have negligible effects. The Single-Loop antenna efficiently couples power at low magneto-static field values (i.e., $B_0 < 100$ G), while the Nagoya Type-III antenna does so at high magneto-static field (i.e., $B_0 > 500$ G) and high bulk plasma density values (i.e., $n_{bulk} = 10^{19}$ m^{-3}).

Abstract Italiano

Una sorgente di plasma Helicon è una sorgente di plasma ad alta densità ed alta efficienza che sostiene una produzione stabile di plasma tramite assorbimento e propagazione di onde helicon. Una tipica sorgente di plasma Helicon è composta da: (i) un sistema di iniezione di gas; (ii) una colonna di plasma a forma cilindrica; (iii) spire magnetiche per il confinamento del plasma; (iv) un'antenna RF che lavora con frequenze attorno al MHz. Le sorgenti di plasma Helicon sono state utilizzate in diversi processi industriali e, ultimamente, anche nel settore della propulsione spaziale. Le cifre di merito propulsive di un HPT (ad es. efficienza di spinta, impulso specifico) dipendono dalla potenza depositata dall'antenna nel plasma, potenza che è proporzionale alla parte reale dell'impedenza di antenna.
In questo lavoro abbiamo indagato la deposizione di potenza da parte di tre diverse antenne RF (ossia la Single-Loop, la Nagoya Type-III e la Fractional Helix) all'interno di un plasma non uniforme, descritto tramite profilo parabolico lungo la direzione radiale e profilo Gaussiano lungo la direzione assiale, come funzione di parametri di scarica di plasma (ad es. densità di bulk e di edge di plasma, temperatura elettronica, pressione dei neutri di background).
Abbiamo utilizzato ADAMANT, uno strumento numerico con approccio elettromagnetico basato su un sistema di equazioni integrali accoppiate di superficie e di volume. Gli intervalli di valori dei parametri di scarica di plasma indagati sono: (i) campo magneto-statico al di sotto di < 1000 G; (ii) densità di bulk di plasma da $10^{18}\ m^{-3}$ a $10^{19}\ m^{-3}$, densità di edge di plasma da $10^{17}\ m^{-3}$ a $5 \times 10^{18}\ m^{-3}$; (iii) temperatura elettronica da 3 eV a 7 eV; (iv) pressione dei neutri di background da 15 mTorr a 30 mTorr.
I risultati mostrano che i profili di densità di plasma influenzano soltanto la magnitudine della parte reale dell'impedenza, mentre l'andamento delle curve di deposizione di potenza come funzioni dei valori di campo magneto-statico è influenzato dal valore di densità di bulk di plasma. I profili radiali e radiali-assiali mostrano simili andamenti di deposizione di potenza per tutte le antenne e i valori dei parametri considerati. La quantità di potenza accoppiata nel plasma dipende anche dal valore di campo magneto-statico e dalla geometria d'antenna, mentre la temperatura elettronica e la pressione dei neutri di background comporta effetti trascurabili. L'antenna Single-Loop è accoppia potenza in modo efficace a bassi valori di campo magneto-statico (ossia $B_0 < 100$ G), mentre l'antenna Nagoya Type-III fa lo stesso per alti valori di campo magneto-statico (ossia $B_0 > 500$ G) e alti valori di densità di bulk di plasma (ossia $n_{bulk} = 10^{19}\ m^{-3}$).

List of Symbols

$\boldsymbol{B}$	magnetic induction	$[G]$
$\boldsymbol{B_0}$	magneto-static field	$[G]$
$\boldsymbol{J}_A$	electric current density	$[A/m^2]$
$\boldsymbol{D}_P$	electric flux density	$[C/m^2]$
Z_A	antenna impedance	$[\Omega]$
λ_0	free space wavelength	$[m]$
f	frequency	$[Hz]$
ω	angular frequency	$[rad/s]$
T_e	electron temperature	$[eV]$
p_n	neutral pressure	$[mTorr]$
n_0	uniform plasma density	$[m^{-3}]$
n_{bulk}	bulk plasma density	$[m^{-3}]$
n_{edge}	edge plasma density	$[m^{-3}]$

List of Acronyms

EM	ElectroMagnetic
RF	Radio-Frequency
TG	Trivelpiece-Gould
$FDFD$	Finite-Difference Frequency-Domain
MoM	Method of Moments
PEC	Perfect Electric Conductor
RWG	Rao-Wilton-Glisson
SWG	Schaubert-Wilton-Glisson

List of Figures

Chapter 1

Introduction

1.1 Helicon plasma source description

A Helicon plasma source is a physical system designed to produce a plasma discharge. This system is mainly composed of four parts: (i) gas source; (ii) cylindrically-shaped plasma column; (iii) magnetic coils; (iv) RF antenna.

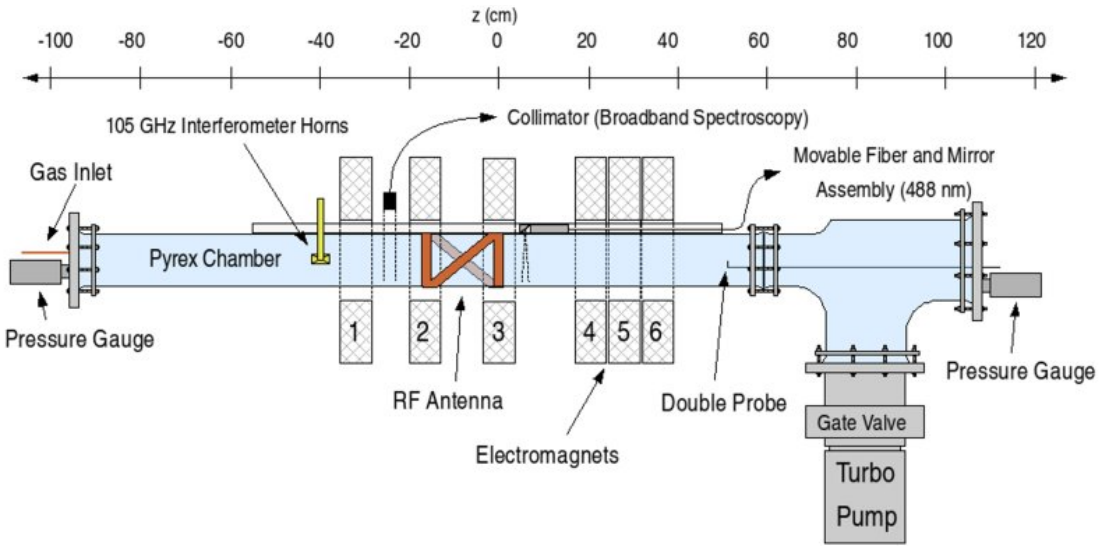

Figure 1.1: Example of Helicon plasma source (MadHeX Helicon Plasma Facility) [1],[2].

As in Fig.1.1, the pumping system generates pressures in the order of the mTorr, allowing the gas to flow from the gas source into the cylindrical shaped tube. The electromagnets generate the confinement by means of a quasi-axial magneto-static field below <1500 G that, along with the physical tube, constrains the plasma within the cylinder. The RF antenna, with working frequency in the range of the MHz, generates Whistler waves which propagate and deposit power, generating and heating the plasma. The probes are used to

measure the various parameters involved, such as magnetic field, pressure, and density.
The main interest in such sources is that with a low amount of power given to the antenna as input, an elevated density in the plasma may be reached, thus making this system very efficient in plasma generation; high densities (up to 10^{19} m^{-3}) are generated employing a magnetic field below <1000 G, using antennas of simple geometry such as the Single-Loop (or *Stix Coil* [3],[4]) and the Nagoya Type-III [5].
The first experiments on gaseous plasma were conducted in 1960 on a toroidal geometry, with probe-like transmitting and receiving antennas [6]. Blevin and Thonemann employed a cylindrical plasma column with an axial magnetic field used as confinement for the plasma, with magneto-static field of 2000 G and the frequency of the antenna varying between 6 - 28 MHz [7]. The cylindrical shape of the plasma container came into account with Lehane and Thonemann, who were the first to study Helicon wave propagation for a magnetic fieldlower than 500 G, 3 kW of generated power for the antenna and the pressure of the Xenon gas between 10 - 70 mTorr [8].
In the late 60's, in Australia, Boswell used a double-loop antenna and a small diameter glass tube, along with axial magnetic fields for physical confinement of the plasma [9]. Only in 1978 the Nagoya Type-III geometry was studied, as a simplification of a double-loop antenna [10].
In the early 80's the Helicon source had been used to simulate the interaction between electron beams and Auroral plasma [11], but with the emerging computer industry the uses have primarily changed to semiconductor processing, including etching and deposition of integrated circuits. Other uses include electrodeless beam sources, laser accelerators and plasma thrusters, the latter being the main interest of this work.
In the years following the first use of the Nagoya Type-III antenna, the Helicon source system had undergone only minor changes, whereas the studies were more focused on the physics of wave propagation and the mechanism leading to power deposition in plasma cylinders.

1.2 Theoretical studies and numerical approaches

The study of Helicon sources can be divided primarily in two parts: propagation of Whistler waves and power deposition, both happening within the plasma cylinder. The RF antenna generates Whistler waves [12], which propagate in the frequency range of $\Omega_{ci} \ll \omega_{LH} \ll \omega \ll \omega_{ce}$, where Ω_{ci} (ω_{ce}) is the ion (electron) cyclotron angular frequency and ω_{LH} is the lower-hybrid frequency.
There has been an ample debate regarding the nature of the propagating waves, whereas the early years involved the study of wave propagation via the dispersion relation. At first, only one type of wave (called "Helicon" and referred to as H) was thought to propagate within the plasma. In 1959 discrepancies between simulations and experimental results found near the plasma cylinder's boundary lead to the idea of a second wave mode (called "Trivelpiece-Gould", referred to as TG [13]) coupled to the Helicon. Nevertheless, it was only in the early 90's that this theory became dominant [12],[14],[15], leading to the complete dispersion relation which reads:

$$\delta\nabla\times\nabla\times\mathbf{B}-k\nabla\times\mathbf{B}+k_w^2\mathbf{B}=0 \tag{1.1}$$

where k is the axial wave number, $\delta=\frac{\omega+i\nu}{\omega_{ce}}$ is a complex factor taking into account the plasma collisionality ν and $k_w^2=\delta k_s^2$, with $k_s=\frac{\omega_p}{c}$ being the skin number. All wave quantities (e.g. $\mathbf{B}$ in Eq.1.1) have an harmonic dependence to time and space in the form of $exp[i(m\theta+kz-\omega t)]$ [12].
Eq.1.1 can be factorized as:

$$(\beta_1-\nabla\times)(\beta_2-\nabla\times)\mathbf{B}=0 \tag{1.2}$$

where β_1 and β_2 are the total wave numbers of the H and TG wave modes, respectively, and are roots of:

$$\delta\beta^2-k\beta+k_w^2=0 \tag{1.3}$$

$$\beta_{1,2}=\frac{k}{2\delta}[1\mp(\,-\frac{4\delta k_w^2}{k^2})^{\frac{1}{2}}]\quad\Rightarrow\quad\beta_1\approx\frac{k_w^2}{k}\ ,\ \beta_2\approx\frac{k}{\delta} \tag{1.4}$$

Moving onto power deposition, there are primarily two means by which the Whistler waves deposit power within the plasma: (i) collisions and (ii) Landau damping. Collisions may be both of mechanical and electromagnetic nature, the former coming from the interaction between charged species and neutral particles, the latter happening between charged particles. The accelerating electrons impact either charged or neutral particles, either way resulting in power deposition. Landau damping is caused by the interaction of electrons and waves propagating in the plasma. A plasma can be defined by the relevance of either of the two processes, thus resulting in a collisional or non-collisional plasma respectively.
Landau damping has been thoroughtly discussed in recent years. The hypothesis of Landau damping as the dominant process in power deposition was first introduced by F.F. Chen in 1991 [16]. As the studies on TG waves progressed, Landau damping became less probable as an explanation for the high densities registered in Helicon discharges [17]. It was but in 1998, after further studies and the discovery of TG waves, that Landau damping has been regarded as a non-predominant cause in power deposition. Instead, as Shamrai *et al.* pointed out, the main cause for power deposition in the plasma is found in the coupling of H and TG wave modes near the plasma cylinder's surface (uniform plasma density case) and volume (non-uniform plasma density case) [18].
Along with physical models a parallel study of numerical codes has been implemented for a better understanding of the physics behind Helicon plasma sources, as well as for power deposition enhancement in the latters. The first study containing a computer code developed and discussed for this purpose, i.e. the *ANTENA* code, has been published in 1996. This tool was originally meant to study ion cyclotron waves, but was later modified for Helicon plasma sources analysis, taking into account the radial density and temperature profiles as well as both Landau and collisional damping. Results have shown that with a small amount of fast electrons the RF power is absorbed mostly via Landau damping [19]. Whitson and Berry later developed *MAXEB* [20], a 2-dimensional (r,z) computer code that examines power absorption in an inhomogeneous cold plasma. The code used the local plasma dielectric tensor in order to calculate the wave fields.
Around 1998 Chen and Arnush adopted a solution based on numerical integration of a

fourth-order ordinary differential equation (ODE) by means of a numerical boundary-value problem regarding radially nonuniform helicon plasmas: their results were implemented in the *HELIC* code [12],[14],[21].
In 1999 Mouzouris and Scharer modified MAXEB [22], resulting in the *ANTENA2* code [23]. The code investigates density profile effects of Helicon plasmas, in regards to wave properties and power absorption, by decomposing EM fields into transverse electric (TE) and transverse magnetic (TM) waveguide modes.
In 2012 Melazzi *et al.* developed the code *SPIREs* (plaSma Padova Inhomogeneous Radial Electromagnetic solver), a fast FDFD numerical tool that calculates the stationary electromagnetic fields propagating in a plasma cylinder in the radial dimension. The code is capable of evaluating the wave propagation and power deposition in magnetized, plasma-filled infinite circular waveguides. The simulations operated by SPIREs can be set for a wide range of frequencies and values of plasma, also including multiple single- or multi-ionised species [24].
In 2014 Melazzi and Lancellotti developed the Fortran code *ADAMANT* (Advanced coDe for Anisotropic Media and ANTennas), designed to study different antenna geometries and their infuence in power deposition in a Helicon plasma source [25]. This very tool is adopted in this work for plasma discharge simulation and analysis.

1.3 Space Propulsion applications

Helicon sources have been used throughout the years in many industrial processes, in particular they were lately employed for space propulsion [26].
From Fig.1.2 we see the different systems involved in a typical Helicon Plasma Thruster (HPT): a gas feeding system, a plasma cylinder, an antenna and an electromagnetic divergent nozzle. The feeding system injects a neutral gas into a dielectric cylindrical chamber, surrounded by an RF antenna working in the MHz range that ionises the neutral gas and heats the resulting plasma. The magnetic coils provide the quasi-axial magnetic field that allows the propagation of Helicon waves and the confinement of plasma within the cylinder. At the exhaust section the topology of the magnetic field becomes divergent, thus providing a "magnetic nozzle" effect on the plasma, which results in the detachment of plasma charged particles and creating thrust in the opposite direction.
The process of thrust generation in a HPT can be divided in two parts: (i) the production stage that occurs in the plasma source and (ii) the acceleration stage at the exhaust section of the thruster. In the former, electrical power is used to ionize the propellant, then kinetic energy is imparted to the plasma via plasma-wave interaction: that leads to the power deposition into the plasma. In the latter, the plasma is exhausted by means of fluid-dynamics and EM processes, leading to supersonic acceleration of plasma and detachment from the magnetic nozzle.
There are three major projects employing Helicon plasma sources for space propulsion: (i) NASA's VASIMR (VAriable Specific Impulse Magnetoplasma Rocket) [27], (ii) the Australian ANU and (iii) the European HPH.com (Helicon Plasma Hydrazine Combined Micro) [28],[29]. In particular, VASIMR couples a plasma source with a second-stage Ion Cyclotron Resonance Heating (ICRH) for ion heating, where the Helicon plasma source is

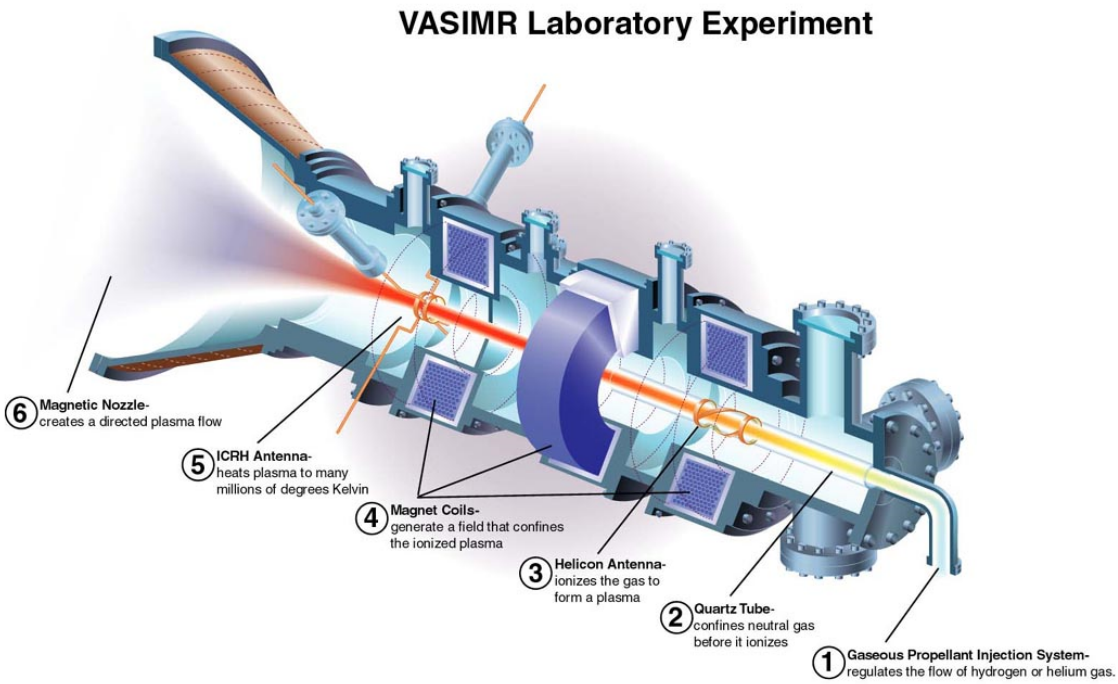

Figure 1.2: VASIMR plasma propulsion system.

the primary ionization source; the HPH.com project is instead thought to design, optimise and develop a space Helicon thruster for small satellites. The thruster class is 50 W - 1 mN. Its application on a mini satellite is thought for attitude and position control. The project also evaluates the possibility to use this system to heat and/or decompose a secondary propellant, to develop a two mode thruster, a high-efficiency low-thrust plasma-thruster mode and a low-efficiency high-thrust secondary-propellant plasma-enhanced mode. To enhance the propulsive figures of merit (thrust, specific impulse and thrust effciency), this project has considered different geometrical source configurations, magnetic field values and topologies, antenna types and feeding frequencies.
Since the propulsive figures of merit depend on the power coupled by the antenna into the plasma [30],[31] and the power deposition is related to the real part of the antenna impedance [25], we have analyzed the influence of the plasma discharge parameters (e.g. plasma density profile, magneto-static field) on the real part of the antenna impedance.

Chapter 2

ADAMANT numerical code

This chapter is meant as a guide the numerical code ADAMANT [25], a full-wave numerical tool that relies on a set of coupled surface and volume integral equations; these governing equations are numerically solved through the MoM approach in the form of Galerkin. The code solves for the surface current density ($\mathbf{J_A}$) on the metal surface S_A, modeled with a triangular-faceted 3D mesh, and for the electric flux density ($\mathbf{D_P}$) in the plasma volume V_P, modeled with a tetrahedral mesh. The unknowns, i.e. J_A and D_P, are expressed as a linear superposition of RWG and SWG functions, respectively [32],[33]. The former is associated with the inner edges of the triangular tessellation and have support on pairs of adjacent triangles; the latter is associated with the facets of the tetrahedral mesh and have support on two tetrahedra if the facets belong to the plasma cylinder volume. Further informations on the EM model and numerical approach can be found in [25].
We distinguished three phases in running ADAMANT, namely preprocessing, numerical solution, and post-processing. We describe the operational process to follow in each phase in order to correctly run a simulation.

2.1 Preprocessing

We draw the geometries of our system through GMSH [34], a free finite element mesh generator. Firstly we draw the plasma volume, then we mesh it in tetrahedral elements. Fig. 2.1 shows an example of plasma column mesh with a plane cut of the plasma cylinder, emphasizing the tetrahedral discretization of the volume.

The mesh size can be controlled by setting the characteristic length of the tetrahedral element for each point drawn in a **.pro* file containing the main mesh and geometry parameters. The mesh is exported as a **.msh* file to be processed by a customized mesh converter. The mesh converter generates a **.vie.msh* file, which is composed of four blocks:

1. The first block contains the vertex information. It is structured in five columns. The first reports the flag 1 identifying the *vertex block*, the second contains a number identifying each vertex, and the last three contain respectively the x, y, and z coordinates of each vertex;

2. The second block contains the triangle information. It is structured in six columns.

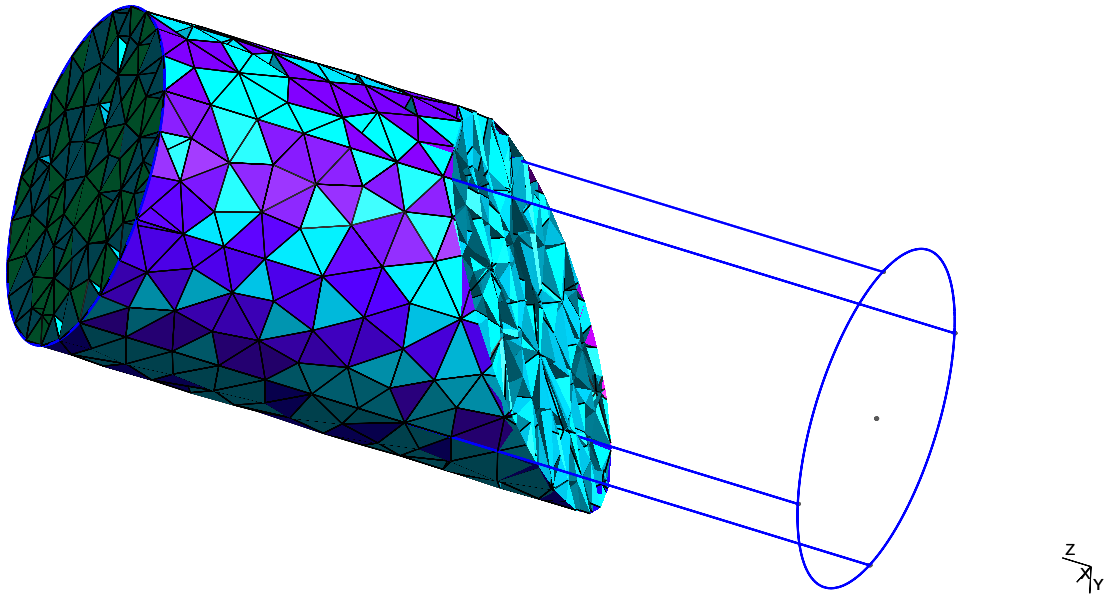

Figure 2.1: Partial plasma column mesh example with a particular of the plasma cylinder mesh, transversely cut.

The first reports flag 2 identifying the *triangle block*, the second contains a number identifying each triangle. The third, fourth, and fifth columns contain the numbers corresponding to the three vertexes composing the triangle, and the sixth reports the area of each triangle;

3. The third block contains the tetrahedron information. It is structured in twenty-two columns. The first reports the flag 3 identifying the *tetrahedron block*, the second contains a number identifying each tetrahedron, the next four columns report the identifying number of the four triangles that compose the tetrahedron, the next three columns report the barycenter coordinates, the tenth reports the tetrahedron volume. The last twelve columns contain the (x, y, z) components of the normals to each facet of the tetrahedron;

4. The fourth block contains the SWG information. It is structured in four columns. The first reports the flag 4 identifying the *SWG block*, the second contains a number identifying each function. The last two columns contains the identifying number of the two adjoining tetrahedrons on which the SWG is defined.

We proceeded in building the antenna assigning PEC material properties to the surface. We mesh the geometry in triangular elements, as shown in Fig. 2.2. We apply (with reference to *voltage gap* source type) the feeding by setting the port region composed by

at least one couple of adjoining triangles. We assign to the two triangles of each couple the port and ground material properties respectively. We can set up to four independent voltages, each a different port region.

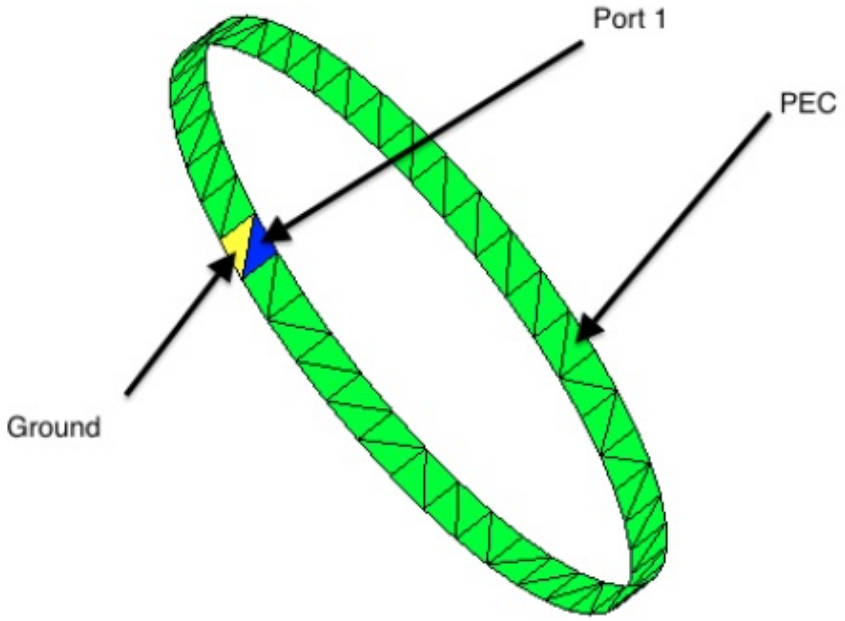

Figure 2.2: Single-Loop antenna mesh example with highlighted PEC (green), Port (blue) and Ground (yellow).

The mesh file has to be exported as **.inp* file and processed by the appropriate mesh converter. The mesh converter generates a **.ant.msh* file which is composed of three blocks:

1. The first contains the vertex information, and it is structured in five columns. The first reports the flag 1 identifying the *vertex block*, the second contains a number identifying each vertex, and the last three columns contain respectively the x, y, and z coordinates of each vertex;

2. The second block contains the triangle information. It is structured in six columns. The first reports the flag 2 identifying the *triangle block*, the second contains a number identifying each triangle, the next three columns report the number of the vertex composing each triangle, and the last column contains a flag identifying the material properties assigned to that triangle. The latter can be 1, -1, 11, 12, 13 or 14, indicating respectively the PEC, ground, port 1, port 2, port 3 or port 4 material properties.

3. The third block contains the RWG information, and it is structured in five columns. The first reports the flag 3 identifying the *RWG block*, the second contains a number

identifying each function, the next two columns report the identifying numbers of the two adjoining triangles on which the RWG is defined.

2.2 Solution

ADAMANT needs four input files to run:

1. the **.vie.msh*;
2. the **.ant.msh*;
3. the *plasma.inp*;
4. the *adamant_data.inp*.

The *adamant_data.inp* file contains the simulation parameters:

```
&geometry
      Sgeoname  = "ANTENNA MESH NAME"
      Vgeoname  = "VOLUME MESH NAME"
/
&settings
      sourcetype = "voltage_gap"
  dieltype = "plasma"
      ntheta = 180
      nphi = 180
  debugging = 0
/
&plasma
      gas = "Ar"
  species = 2
      Bzconf = 0
  Npress = 1.5d1
  profile = 1
  Spow    = 2
  Tpow    = 1
  nedge   = 1.000000d+17
/
&param
      nports   = 1
/
&impedance
      Zref(1) = 50.0d0
      Zref(2) = 50.0d0
      Zref(3) = 50.0d0
      Zref(4) = 50.0d0
```

```
/
&feeding
      voltages(1) = (1.0d0,0.0d0)
      voltages(2) = (1.0d0,0.0d0)
      voltages(3) = (1.0d0,0.0d0)
      voltages(4) = (1.0d0,0.0d0)
/
&frequency
      fsim = 15d6
      dcellmax = 0.25
/
&Sintegration
      d_threshold = 3.0d0
      ord1(1:2) = 4 4
      ord2(1:2) = 4 4
      ord3(1:2) = 4 4
      ord4(1:2) = 4 4
/
&Vintegration
      sord1(1:2) = 1 3
      sord2(1:2) = 1 3
      sord3(1:2) = 3 4
      sord4(1:2) = 3 4
      vord1(1:2) = 1 3
      vord2(1:2) = 1 3
      vord3(1:2) = 3 4
      vord4(1:2) = 3 4
/
&background
      epr = (1.0d0,0.0d0)
      mur = (1.0d0,0.0d0)
/
```

As shown above, the file is composed by ten blocks, each regarding simulation parameters grouped as follows:

geometry regards the geometry files, and it has to be completed with the mesh converted file names, for the surface and volume respectively;

settings is about simulation settings and it contains:

1. the source type, that can be *plain_wave* or *voltage_gap*. When the source type is set as *voltage_gap*, the code needs the ground and port material properties in the mesh converted file;
2. the dielectric type that can be *dielectric* or *plasma*. The code needs respectively a *dielectric.inp* or *plasma.inp* file to run.

3. the number of ϕ samplings, where the electric fields are evaluated in the far field region;
4. the number of θ samplings, where the electric fields are evaluated in the far field region;

plasma regards the plasma and it contains:

1. a gas flag (the element symbol) which can be *Ar*, *N2*, *H2*, *He* or *Ne*;
2. the number of species;
3. the magneto-static field intensity $[T]$;
4. the neutral background pressure $[mTorr]$;
5. a flag for non-uniform density profile enabling;
6. the integer number s from the $n(s,t,r)$ non-uniform density profiles;
7. the integer number t from the $n(s,t,r)$ non-uniform density profiles;
8. the edge plasma density profile $[m^{-3}]$;

param reports the number of ports set in the excitation circuit geometry;

impedance is the reference impedance for each port $[\Omega]$; it contains four complex numbers, one for each port;

voltages is the voltage gap feeding each port $[V]$;

frequency is divided into two rows. The first reports the simulation working frequency $[Hz]$, while the second is a threshold parameter for the code;

Sintegration defines the surface numerical integration formulas;

Vintegration defines the volume numerical integration formulas;

background reports the electric permittivity ε $[F/m]$, and the magnetic permeability μ $[H/m]$ of the background medium.

The *plasma.inp* file contains the plasma species informations:

```
#species
      "electrons"
  -1.602176462d-19
  9.10938188d-31
  1.0d+19
  3.000000d+00
  1
#
#species
      "ions"
  +1.602176462d-19
```

```
  6.63367652e-26
  1.0d+19
  3.0000000d-02
  1
#
```

The *plasma.inp* file is structured in two blocks, one for each species. Each block is composed by six rows:

1. the name of the species considered in the block;
2. the charge $[C]$;
3. the mass $[Kg]$;
4. the uniform density (uniform plasma density case) or the bulk density (non-uniform plasma density case) $[m^{-3}]$;
5. the temperature $[eV]$;
6. a flag representing the plasma collisionality, that can be either 1 if the plasma is collisional, or 0 if it is not.

2.3 Running and postprocessing

ADAMANT can be run by typing

```
> ./adamant
```

on the command line.
ADAMANT generates four output files:

adamant_PEC_Ja.txt reports the current distributed on the metal surface. It is composed by four columns. The first column reports the port number associated with that solution of the EM problem, the second is the RWG identifying number, and the last two indicate respectively the real, and imaginary part of the current for each function.

adamant_PEC_param.txt contains the real and imaginary parts of the admittance, impedance, S parameters (from the dielectric tensor) for each port combination, and the input power in different blocks. Each block is composed of four columns, the first two reporting the ports associated with the solution and the last two respectively the real and imaginary parts of the parameter considered. In the input power block, the first two columns report the value 0.

adamant_DIELECTRIC_D.txt reports the current distribution in the plasma volume. It is structured in four columns. The first column reports the port number associated with the solution of the EM problem, the second is the SWG identifying number, and the last two indicate respectively the real, and imaginary part of the current for each function.

Es_farzone.txt contains the electric far field intensity evaluated in the (θ, ϕ) coordinates point in the far field region.

Customized MATLAB scripts have also been developed to load simulation output data and specifically to produce plots in a suitable form; in particular, a script was developed in order to load the input impedance from the file *adamant_PEC_param.txt*, and then plot the impedance as a function of plasma discharge parameters (e.g. plasma density, neutral background pressure, magneto-static field).

Chapter 3

Sensibility analysis

The accuracy of the numerical results depends on the number of basis functions used, respectively, for the description of the current distribution density on the antenna surface (i.e. RWG functions) and the total electric flux density in the plasma volume (i.e. SWG functions). The higher the number of basis functions the better the distribution of the unknowns can be represented, but also the longer the computational time, and the risk of incurring in numerical instabilities related to the dimensions of triangular and tetrahedral elements [25].

3.1 Driving parameters

The dominant parameters in the RWG and SWG number assessment are: (i) the working frequency f; (ii) the antenna geometry; (iii) the plasma discharge parameters. Since the RWG and SWG basis functions are defined on triangular and tetrahedral elements respectively, the requirements on their number may be translated into the following rules of thumb:

a. At least 10 mesh element per wavelenght λ_0;

b. The triangular patches on the antenna should be as similar as possible to their corresponding in the plasma volume.

Since the focus of this work is the effect of plasma density profiles on the real part of the antenna impedance, the latter needs to be correctly described by using a suitable number of basis functions. In regards to the antenna mesh, since λ_0 is in the order of tens of meters and the antenna characteristic dimensions are in the order of a few centimeters, we have chosen the number of RWG basis functions to correctly represent the geometry of each antenna. The number of RWG basis functions has been reported in Tab.3.1 for each antenna. Therefore we have investigated the antenna impedance as a function of different SWG numbers. We have considered a plasma mesh with a number of SWG basis functions ranging from ~ 5000 to ~ 25000.

Antenna Type	RWG functions
Single-Loop	72
Nagoya Type-III	770
Fractional Helix	748

Table 3.1: Antenna meshes andnumber of RWG basis functions.

We have performed the numerical analysis both in the uniform and the non-uniform plasma density configurations. In the former the plasma density is set to 10^{19} m^{-3}; in the latter we have considered a radial density profile $n(2, 1, r)$ with bulk density of 10^{19} m^{-3}, and edge density of 10^{18} m^{-3} and a density profile along the radial and axial directions with the same bulk and edge values as for the radial configuration. In both the uniform and non-uniform cases the plasma is magnetized with axial magneto-static field of 300 G, and plasma discharge parameters $T_e = 5$ eV and $p_n = 15$ mTorr.

3.2 Results

We have considered both the real and the imaginary part of the antenna impedance (Z_A) as a function of the number of SWG basis functions in the uniform plasma density case (Fig.3.1), in the non-uniform radial (Fig.3.2) and non-uniform radial-axial (Fig.3.3) density cases.
Regarding the real part of the impedance, in Figs.3.1(a),3.2(a),3.3(a) the Single-Loop and the Fractional Helix antennas show an asymptotic behaviour for each analyzed case, whereas the Nagoya Type-III antenna exhibits a decreasing tendency as the SWG number increases (with an exception in the uniform case).
Regarding the imaginary part of the antenna impedance (see Figs.3.1(b),3.2(b),3.3(b)), the trends are almost horizontal. This suggest that the imaginary part of the impedance is less affected by the number of SWG functions.
According to these results and to the rules of thumb, since the impedance variations are overall small compared to the order of magnitude of the real part of the impedance, we have used a plasma mesh with 15448 SWG basis functions to perform the simulations relevant for the physical investigations.

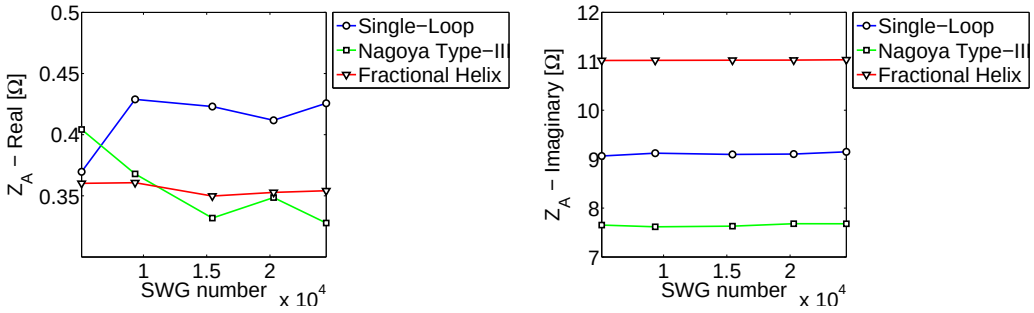

(a) (b)

Figure 3.1: (a) Real and (b) imaginary part of the antennas impedance as function of the SWG number. The antennas (i.e., Single-Loop, Nagoya Type-III, Fractional Helix) drive a uniform ($n_0 = 10^{19}\ m^{-3}$) and magnetized ($B_0 = 300$ G) plasma. Plasma discharge parameters are: $T_e = 5$ eV, $p_n = 15$ mTorr.

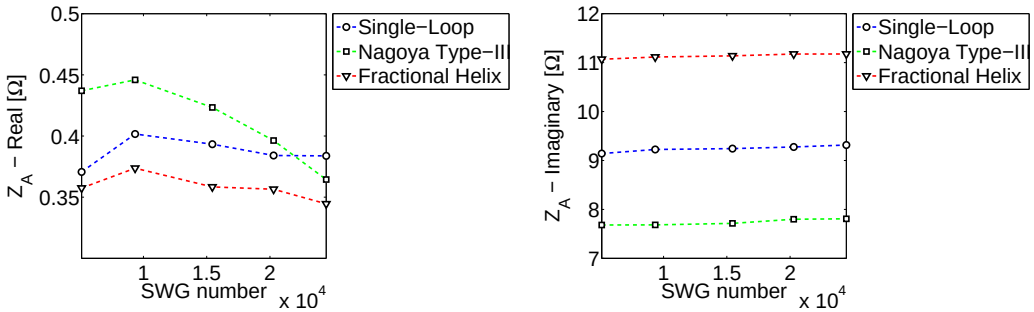

(a) (b)

Figure 3.2: (a) Real and (b) imaginary part of the antennas impedance as function of the SWG number. The antennas (i.e., Single-Loop, Nagoya Type-III, Fractional Helix) drive a non-uniform ($n(2, 1, r)$ density profile , $n_{bulk} = 10^{19}\ m^{-3}$, $n_{edge} = 10^{18}\ m^{-3}$) and magnetized ($B_0 = 300$ G) plasma. Plasma discharge parameters are: $T_e = 5$ eV, $p_n = 15$ mTorr.

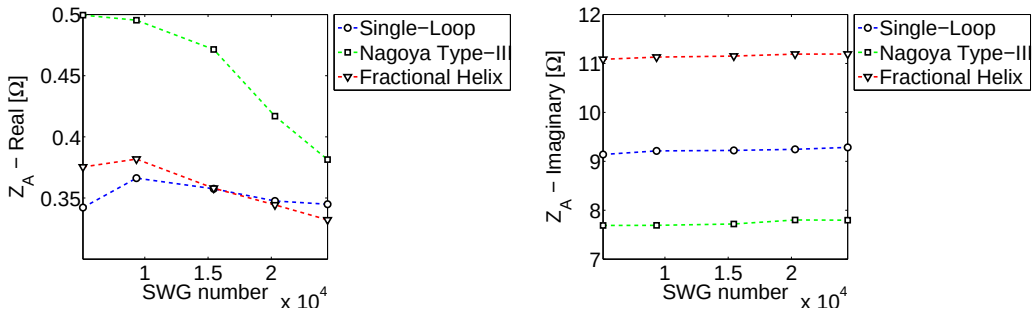

(a) (b)

Figure 3.3: (a) Real and (b) imaginary part of the antennas impedance as function of the SWG number. The antennas (i.e., Single-Loop, Nagoya Type-III, Fractional Helix) drive a non-uniform ($n(2,1,r,z)$ density profile , $n_{bulk} = 10^{19}\ m^{-3}$, $n_{edge} = 10^{18}\ m^{-3}$) and magnetized ($B_0 = 300$ G) plasma. Plasma discharge parameters are: $T_e = 5$ eV, $p_n = 15$ mTorr.

Chapter 4

Power Deposition Analysis

Since the uniform plasma density case has been analyzed in previous works [35], we have focused on a non-uniform plasma discharge. We have analyzed a non-uniform Helicon plasma source with plasma density profiles along the radial and the radial-axial directions, respectively. We have studied the real part of the antenna impedance as a function of different antenna and plasma discharge parameters.

4.1 Non-uniform Helicon source

We have considered a cylindrically-shaped plasma column with radius $b = 0.02$ m and length $L = 0.1$ m. The power is coupled into the plasma by three RF antennas commonly used in Helicon plasma sources discharge, i.e. the Single-Loop, the Nagoya Type-III and the Fractional Helix. Each antenna is placed symmetrically around the plasma and is built as in Fig.4.1, the main geometrical dimensions being: radius $a = 0.03$ m; metallic strips width $w = 0.004$ m for the Single-Loop and $w = 0.006$ m for the Nagoya Type-III and Fractional Helix; Nagoya Type-III and Fractional Helix lenght $L_A = 0.05$ m.
In running simulations with ADAMANT, the number of SWG basis functions we used to represent $\mathbf{D}_P$ is $N_P = 15448$, as a result of the sensibility analysis in Chapter 3. The number N_A of RWG basis functions employed to represent $\mathbf{J}_A$ depends on the examined antenna; specifically, for the Single-Loop $N_A = 72$, for the Nagoya Type-III $N_A = 770$ and for the Fractional Helix $N_A = 748$ (see Tab. 3.1).

Parameter	Values
$B_0\ [G]$	$0:10:50\ ,\ 100:100:1000$
$f\ [MHz]$	15
$(n_{bulk}, n_{edge})\ [m^{-3}, m^{-3}]$	$(10^{18}, 10^{17})\ ,\ (10^{18}, 5\times10^{17})\ ,\ (10^{19}, 10^{18})\ ,\ (10^{19}, 5\times10^{18})$
$T_e\ [eV]$	$3\ ,\ 7$
$p_n\ [mTorr]$	$15\ ,\ 30$

Table 4.1: Plasma discharge parameters.

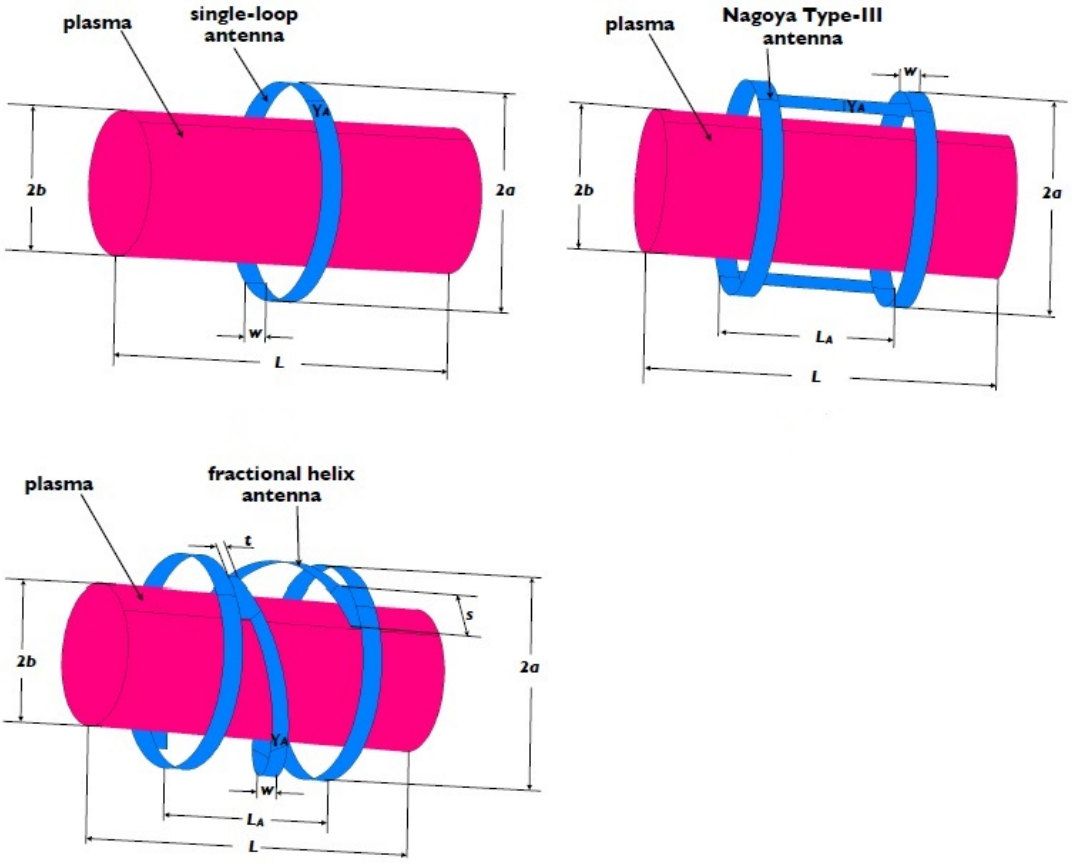

Figure 4.1: Employed plasma and antennas geometry.

We have considered a non-uniform Helicon plasma discharge with both radial and axial density profiles. The varying discharge parameters are: (i) the magneto-static field (B_0); (ii) the bluk plasma density (n_{bulk}); (iii) the egde plasma density (n_{edge}); (iv) the electron temperature (T_e); (v) the neutral pressure (p_n). The range of values are reported in Table 4.1 . The magneto-static field values ranging from 100 G to 1000 G were chosen as typically investigated B_0 values in Helicon plasma discharge analysis [25],[35],[36]. We have also considered low magneto-static field values in the range from 0 G to 50 G since previous works evidenced a peak in the power deposition [37].
The radial density profile is parametrized as follows [14],[24]:

$$n(s,t,r) = n_{bulk}\left[1 - \left(\frac{r}{w}\right)^s\right]^t \tag{4.1}$$

$$w = \frac{b}{\left[1 - f_a^{\frac{1}{t}}\right]^{\frac{1}{s}}} \quad , \quad f_a = \frac{n_{edge}}{n_{bulk}} \tag{4.2}$$

where b is the plasma cylinder radius, r is the radial coordinate and s, t are integer numbers.

The plasma profile along the radial and axial directions is parametrized as:

$$n(s,t,r,z) = n(s,t,r)\ e^{-\frac{z}{L}^2} \tag{4.3}$$

where z is the axial coordinate and L is the plasma column lenght.

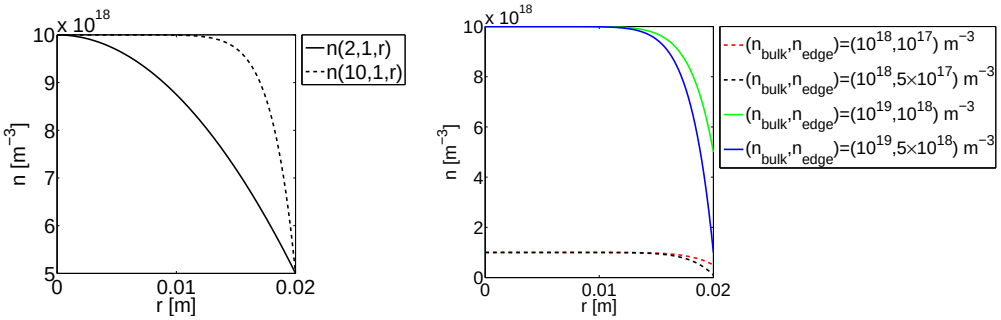

(a) (b)

Figure 4.2: (a) Analyzed radial density profiles and (b) $n(10,1,r)$ profile with different values of plasma density at the bulk and edge, correspondingly.

In this work, we have considered $n(2,1,r)$ and $n(10,1,r)$ profiles (see Fig.4.2(a)) as frequently found profiles in experimental analysis. The former describes plasma density as smoothly decreasing from the bulk value to the edge of the discharge, while the latter features a bulk value almost constant until the edge where the density decreases sharply. Regarding the non-uniform case with density profiles along the radial and axial directions, we have considered the same profiles as above (i.e. $n(2,1,r)$ and $n(10,1,r)$) with a Gaussian profile along the axial direction.
For each profile we have considered different bulk and edge plasma densities (Fig.4.2(b)). As a matter of fact, previous works [36] showed that different bulk density values (e.g. $10^{18}\ m^{-3}$ and $10^{19}\ m^{-3}$) lead to very different physical systems in terms of antenna impedance and power deposition. As pictured in Fig.4.2(b), we have considered different edge density values. It is expected that this changes the wave propagation phenomena in the Helicon source and, by the same token, in the power deposition.

4.2 Analysis of plasma density profiles

4.2.1 Effect of radial and radial-axial profiles

We have investigated the effects of plasma density profiles. In order to enhance the difference between profiles we have reported the results for the same antenna geometry, the bulk-edge values, the electron temperature, and the neutral pressure.To better evidence the effect of plasma density profiles, we have plotted the uniform density values corresponding to the highest and lowest density values met in the non-uniform cases considered.
Figs.4.3,4.4,4.5 show that each antenna performs better with $n(10,1,r)$ and $n(10,1,r,z)$ plasma density profiles rather than $n(2,1,r)$ and $n(2,1,r,z)$ profiles. The non-uniform curves are close to the uniform curves corresponding to $n_0 = 10^{18}\ m^{-3}$ (see Figs.4.3(a),4.4(a),

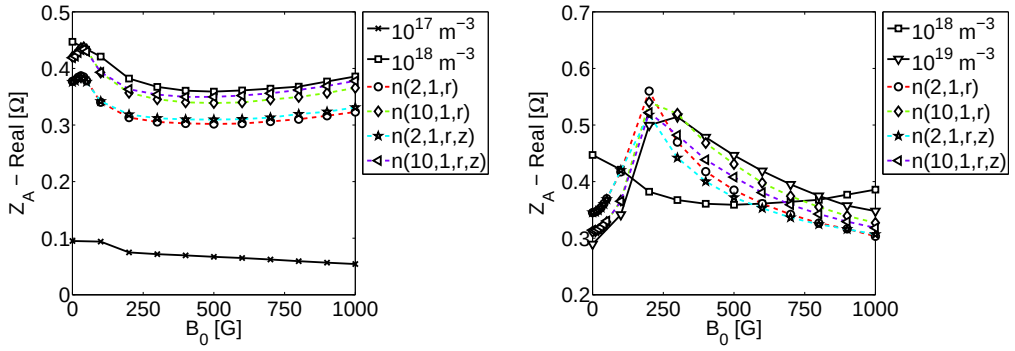

(a) (b)

Figure 4.3: Real part of the impedance of a Single-Loop antenna as a function of the magneto-static field values, and $n(s, 1, r)$, $n(s, 1, r, z)$ plasma density profiles. The antenna works at 15 MHz and drives a non-uniform Helicon plasma source with $T_e = 7$ eV, $p_n = 30$ mTorr, and bulk-edge density values of: (a) $(10^{18}, 5 \times 10^{17})$ m^{-3}; (b) $(10^{19}, 5 \times 10^{18})$ m^{-3}.

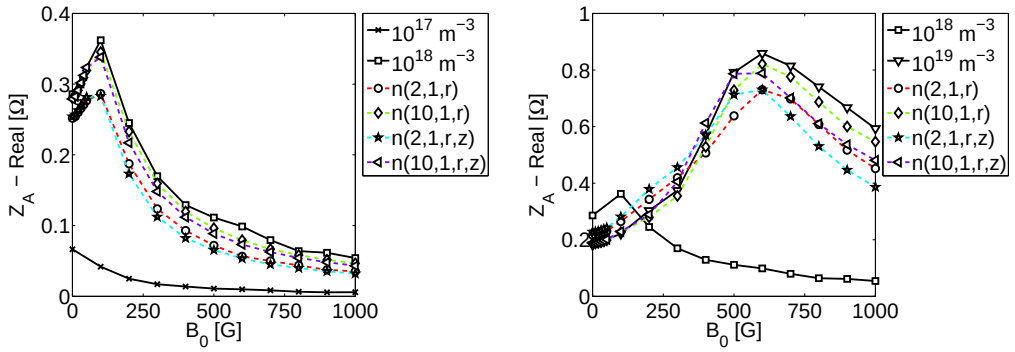

(a) (b)

Figure 4.4: Real part of the impedance of a Nagoya Type-III antenna as a function of the magneto-static field values, and $n(s, 1, r)$, $n(s, 1, r, z)$ plasma density profiles. The antenna works at 15 MHz and drives a non-uniform Helicon plasma source with $T_e = 7$ eV, $p_n = 30$ mTorr, and bulk-edge density values of: (a) $(10^{18}, 5 \times 10^{17})$ m^{-3}; (b) $(10^{19}, 5 \times 10^{18})$ m^{-3}.

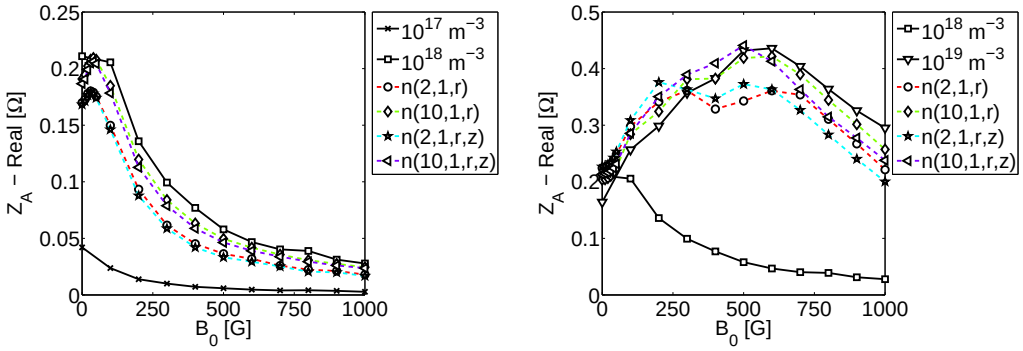

Figure 4.5: Real part of the impedance of a Fractional Helix antenna as a function of the magneto-static field values, and $n(s,1,r)$, $n(s,1,r,z)$ plasma density profiles. The antenna works at 15 MHz and drives a non-uniform Helicon plasma source with $T_e = 7$ eV, $p_n = 30$ mTorr, and bulk-edge density values of: (a) $(10^{18}, 5\times10^{17})$ m^{-3}; (b) $(10^{19}, 5\times10^{18})$ m^{-3}.

4.5(a)) and $n_0 = 10^{19}$ m^{-3} (see Figs.4.3(b),4.4(b),4.5(b)), respectively.
The Single-Loop antenna enhances power deposition at $B_0 \sim 50$ G when driving a plasma with bulk density value of 10^{18} m^{-3} and edge density value of 5×10^{17} m^{-3} (see Fig.4.3(a)). With a bulk density value of 10^{19} m^{-3} and an edge density value of 5×10^{18} m^{-3} (see Fig.4.3(b)), the Single-Loop antenna couples power most efficiently at $B_0 \sim 200$ G.
Figs.4.4(a),4.5(a) show that the Nagoya Type-III and the Fractional Helix antennas enhance power deposition at magneto-static field values below < 100 G, performing best with a $n(10,1,r)$ density profile. With a bulk density value of 10^{19} m^{-3} and an edge density value of 5×10^{18} m^{-3}, the Nagoya Type-III and the Fractional Helix antennas (see Figs.4.4(b),4.5(b)) deposit power most efficiently at $B_0 \sim 600$ G. For magneto-static field values below < 600 G the antennas perform best with a $n(10,1,r,z)$ density profile. At higher magneto-static field values > 600 G the Nagoya Type-III and the Fractional Helix couple power efficiently with the $n(10,1,r)$ profile.

4.2.2 Effect of the bulk and edge plasma densities

To fully understand the role of plasma profiles effects, we have investigated the power deposition with different bulk-edge density values. We have plotted the results for the same antenna geometry, density profile, electron temperature and neutral pressure.
Figs.4.6,4.7,4.8 show that different edge density values have little effect on power coupling, but also that each antenna deposits power more efficiently the greater the difference in value between bulk and edge density values. The non-uniform plasma density curves corresponding to the same bulk density values are well separated in the $n(2,1,r)$ density profile case (see Figs.4.6(a),4.7(a),4.8(a)), while they get closer when considering a $n(10,1,r)$ profile (see Figs.4.6(b),4.7(b),4.8(b)). For each antenna (e.g., see Figs.4.6(a),4.6(b)), the plasma density profile does not affect the trend of the real part of the impedance.
At bulk density values of 10^{18} m^{-3} and edge values of 10^{17} m^{-3} and 5×10^{17} m^{-3}, each antenna shows enhanced power deposition at magneto-static field values below < 100 G. At

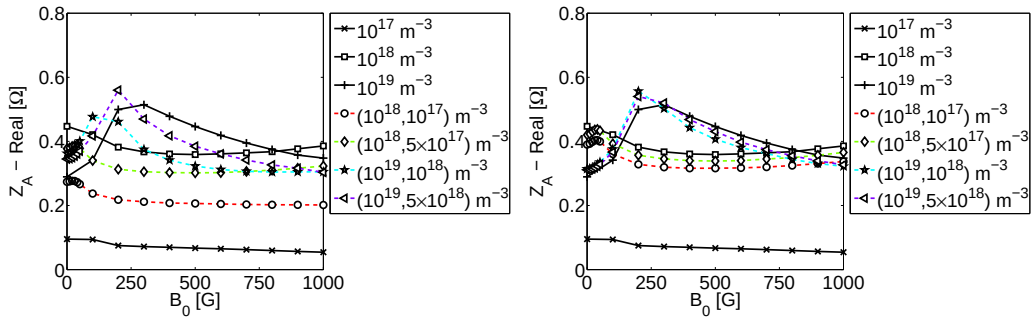

(a) (b)

Figure 4.6: Real part of the impedance of a Single-Loop antenna as a function of the magneto-static field and bulk-edge plasma density values. The antenna works at 15 MHz and drives a non-uniform Helicon plasma source with $T_e = 7$ eV, $p_n = 30$ mTorr, and (a) $n(2, 1, r)$, (b) $n(10, 1, r)$ density profiles.

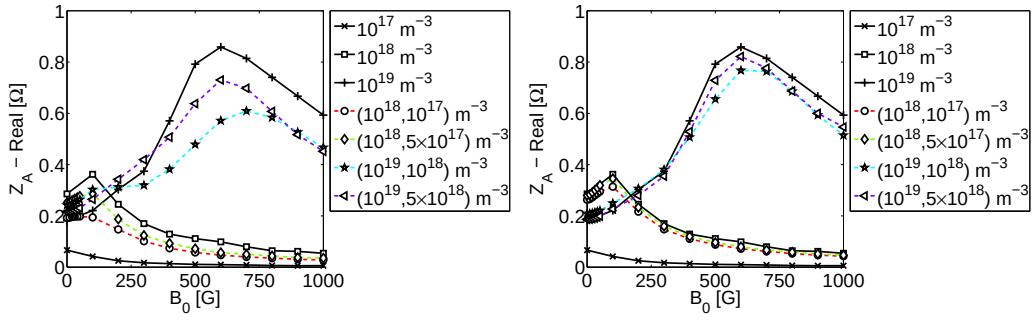

(a) (b)

Figure 4.7: Real part of the impedance of a Nagoya Type-III antenna as a function of the magneto-static field and bulk-edge plasma density values. The antenna works at 15 MHz and drives a non-uniform Helicon plasma source with $T_e = 7$ eV, $p_n = 30$ mTorr, and (a) $n(2, 1, r)$, (b) $n(10, 1, r)$ density profiles.

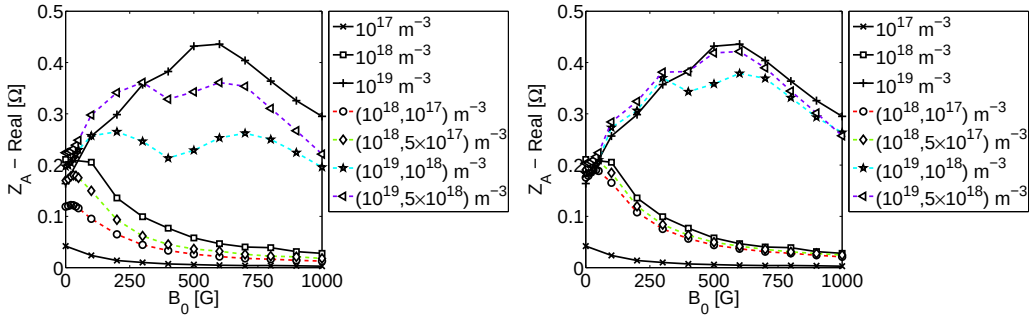

(a) (b)

Figure 4.8: Real part of the impedance of a Fractional Helix antenna as a function of the magneto-static field and bulk-edge plasma density values. The antenna works at 15 MHz and drives a non-uniform Helicon plasma source with $T_e = 7$ eV, $p_n = 30$ mTorr, and (a) $n(2, 1, r)$, (b) $n(10, 1, r)$ density profiles.

bulk density values of 10^{19} m^{-3} and edge density values of 10^{18} m^{-3} and 5×10^{18} m^{-3} the real part of the Single-Loop antenna peaks at $B_0 \sim 200$ G (see Figs.4.6), while the Nagoya Type-III (see Fig.4.7) and the Fractional Helix (see Fig.4.8) antennas deposit power most efficiently at $B_0 \sim 600$ G.

4.3 Effect of the electron temperature

In this section we report the effect of the electron temperature on power deposition in a non-uniform Helicon source.

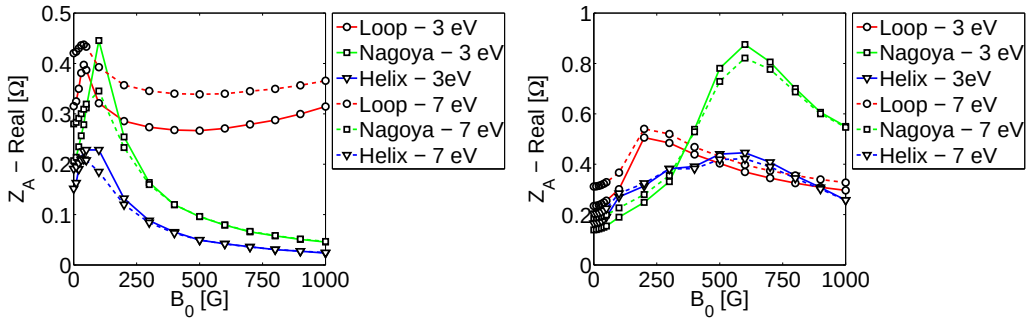

(a) (b)

Figure 4.9: Real part of the impedance of a Single-Loop, a Nagoya Type-III and a Fractional Helix antenna as a function of the magneto-static field. The antennas work at 15 MHz and drive a Helicon plasma source with $n(10, 1, r)$ plasma density profile and bulk-edge pairs of: (a) $(10^{18}, 5 \times 10^{17})$ m^{-3}; (b) $(10^{19}, 5 \times 10^{18})$ m^{-3}. The neutral pressure is $p_n = 30$ mTorr.

For a given density profile, e.g. the $n(10, 1, r)$ (see Fig.4.9(a)), the power deposition curves for a Single-Loop antenna corresponding to $T_e = 3$ eV and $T_e = 7$ eV are well

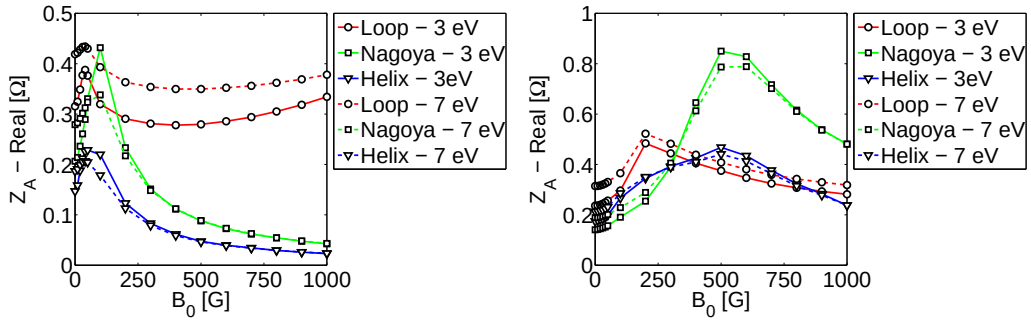

(a) (b)

Figure 4.10: Real part of the impedance of a Single-Loop, a Nagoya Type-III and a Fractional Helix antenna as a function of the magneto-static field. The antennas work at 15 MHz and drive a non-uniform Helicon plasma source $n(10, 1, r, z)$ plasma density profile and bulk-edge pairs of: (a) $(10^{18}, 5 \times 10^{17})\ m^{-3}$; (b) $(10^{19}, 5 \times 10^{18})\ m^{-3}$. The neutral pressure is $p_n = 30$ mTorr.

separated when considering a bulk density value of $10^{18}\ m^{-3}$ and an edge density value of $5 \times 10^{17}\ m^{-3}$; the curves get closer when considering a bulk density value of $10^{19}\ m^{-3}$ and an edge density value of $5 \times 10^{18}\ m^{-3}$ (see Fig.4.9(b)). Regardless of the plasma density profile and bulk and edge density values, the Single-Loop is the most efficient antenna in coupling power into a 3 eV plasma.
At low bulk-edge density values, i.e. $n_{bulk} = 10^{18}\ m^{-3}$ and $n_{edge} = 5 \times 10^{17}\ m^{-3}$ (see Figs.4.9(a),4.10(a)), the power deposition curves of the Nagoya Type-III and the Fractional Helix antennas are well separated for magneto-static field values below < 200 G, becoming overlapped for $B_0 > 300$ G.
At higher bulk-edge density values, i.e. $n_{bulk} = 10^{19}\ m^{-3}$ and $n_{edge} = 5 \times 10^{18}\ m^{-3}$ (see Figs.4.9(b),4.10(b)), the Nagoya Type-III and the Fractional Helix antennas deposit more power with $T_e = 3$ eV for magneto-static field values below < 300 G; the opposite can be found for $B_0 > 300$ G.

4.4 Effect of the neutral pressure

In this section we report the effect of the neutral pressure on power deposition in a non-uniform Helicon source.
For a given density profile, e.g. the $n(10, 1, r, z)$ (see Fig.4.12(a)), the power deposition curves for a Single-Loop antenna corresponding to $p_n = 15$ mTorr and $p_n = 30$ mTorr are well separated when considering a bulk density value of $10^{18}\ m^{-3}$ and an edge density value of $5 \times 10^{17}\ m^{-3}$; the curves get closer when considering a bulk density value of $10^{19}\ m^{-3}$ and an edge density value of $5 \times 10^{18}\ m^{-3}$ (see Fig.4.12(b)). Regardless of the plasma density profile and bulk and edge density values,the Single-Loop is the most efficient antenna in coupling power into a 15 mTorr plasma.
At low bulk-edge density values, i.e. $n_{bulk} = 10^{18}\ m^{-3}$ and $n_{edge} = 5 \times 10^{17}\ m^{-3}$ (see Figs.4.11(a),4.12(a)), the power deposition curves of the Nagoya Type-III and the Frac-

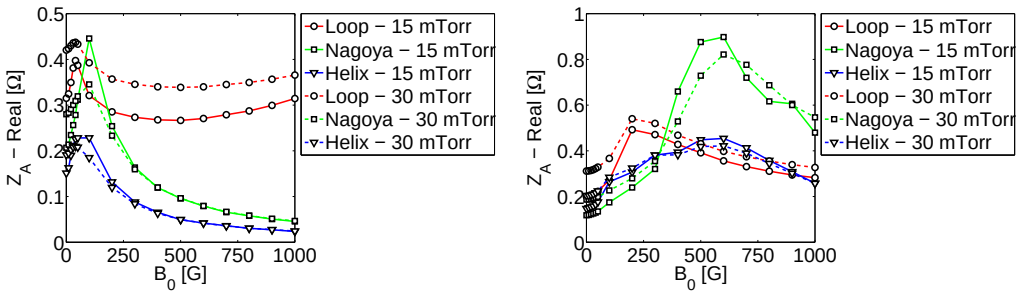

(a) (b)

Figure 4.11: Real part of the impedance of a Single-Loop, a Nagoya Type-III and a Fractional Helix antenna as a function of the magneto-static field. The antennas work at 15 MHz and drive a non-uniform Helicon plasma source with $n(10, 1, r)$ plasma density profile and bulk-edge pairs of: (a) $(10^{18}, 5 \times 10^{17})$ m^{-3}; (b) $(10^{19}, 5 \times 10^{18})$ m^{-3}. The electron temperature is $T_e = 7$ eV.

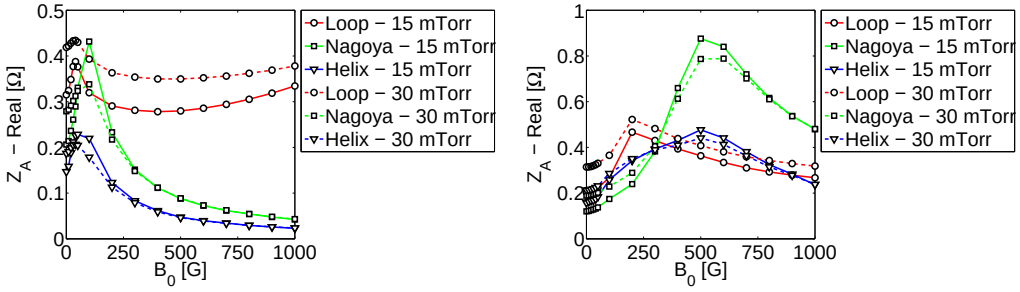

(a) (b)

Figure 4.12: Real part of the impedance of a Single-Loop, a Nagoya Type-III and a Fractional Helix antenna as a function of the magneto-static field. The antennas work at 15 MHz and drive a non-uniform Helicon plasma source with $n(10, 1, r, z)$ plasma density profile and bulk-edge pairs of: (a) $(10^{18}, 5 \times 10^{17})$ m^{-3}; (b) $(10^{19}, 5 \times 10^{18})$ m^{-3}. The electron temperature is $T_e = 7$ eV.

tional Helix antennas are well separated for magneto-static field values below < 200 G, becoming overlapped for $B_0 > 300$ G.
At higher bulk-edge density values, i.e. $n_{bulk} = 10^{19}\ m^{-3}$ and $n_{edge} = 5 \times 10^{18}\ m^{-3}$ (see Figs.4.11(b),4.12(b)), the Nagoya Type-III antenna deposits more power at $p_n = 15$ mTorr for magneto-static field values below < 300 G, regardless of the density profile; the same applies for magneto-static field values $B_0 > 600$ G when considering a $n(10, 1, r)$ profile (see Fig.4.11(b)). For the same bulk and edge density values and $B_0 < 300$ G the Fractional Helix antenna couples power more efficiently into a 15 mTorr plasma; the opposite can be found for magneto-static field values $B_0 > 300$ G.

4.5 Comparison between different antennas

In this section we have plotted the real part of the impedance of each antenna as a function of the investigated magneto-static field values. Results are referred to $(10^{18}, 10^{17})\ m^{-3}$ and $(10^{19}, 10^{18})\ m^{-3}$ bulk-edge plasma density values, $n(2, 1, r)$ and $n(2, 1, r, z)$ plasma density profiles and $T_e = 7$ eV, $p_n = 30$ mTorr.

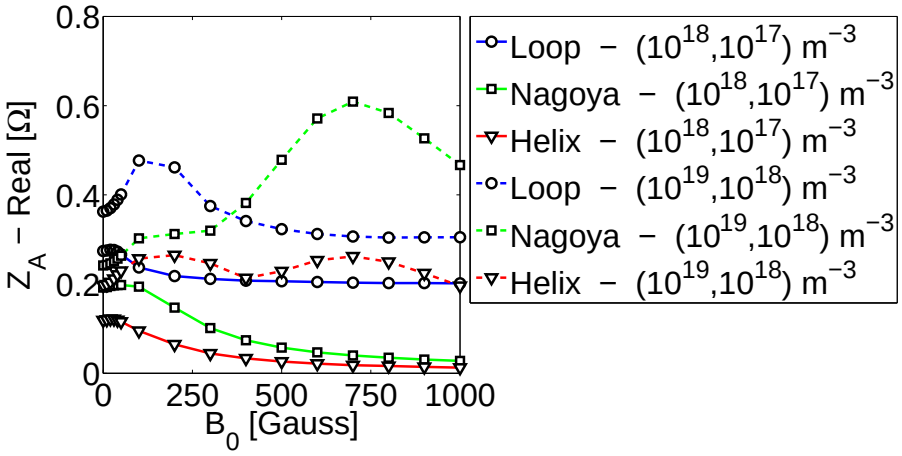

Figure 4.13: Real part of the impedance of a Single-Loop, a Nagoya Type-III and a Fractional Helix antenna as a function of the magneto-static field. The antennas work at 15 MHz and drive a non-uniform Helicon plasma source with $n(2, 1, r)$ plasma density profile and bulk-edge pairs of $(10^{18}, 10^{17})\ m^{-3}$ and $(10^{19}, 10^{18})\ m^{-3}$. Plasma discharge parameters are: $T_e = 7$ mTorr , $p_n = 30$ mTorr.

Considering a plasma with radial density profile (see Fig.4.13), bulk density value of $10^{18}\ m^{-3}$ and edge density value of $10^{17}\ m^{-3}$, each antenna couples power most efficiently at magneto-static field values below < 100 G, where the Single-Loop antenna performs the best. At a bulk-edge value of $(10^{19}, 10^{18})\ m^{-3}$ and for magneto-static field values below < 300 G, the Single-Loop is still the most efficient antenna in coupling power. Above > 300 G the Nagoya Type-III couples power efficiently compared to other antennas, with a peak value around $B_0 \sim 600$ G.
The radial-axial density profile (see Fig.4.14) has a minor effect on both the power depo-

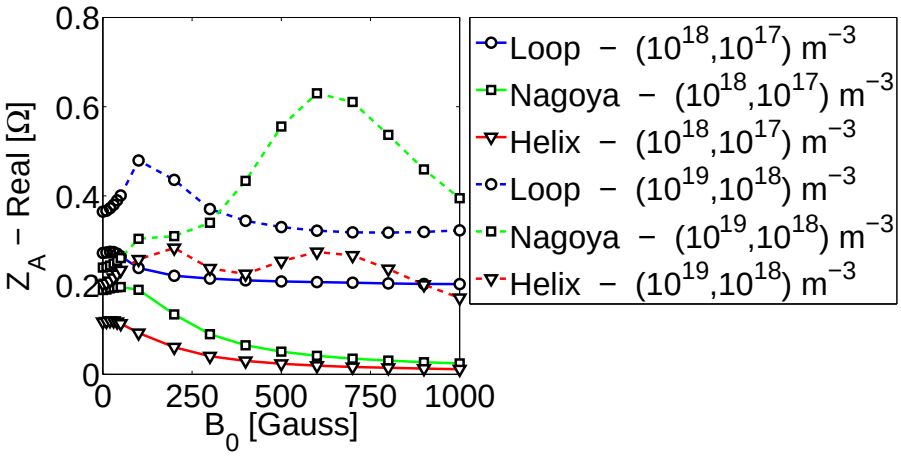

Figure 4.14: Real part of the impedance of a Single-Loop, a Nagoya Type-III and a Fractional Helix antenna as a function of the magneto-static field. The antennas work at 15 MHz and drive a non-uniform Helicon plasma source with $n(2, 1, r, z)$ plasma density profile and bulk-edge pairs of $(10^{18}, 10^{17})$ m^{-3} and $(10^{19}, 10^{18})$ m^{-3}. Plasma discharge parameters are: $T_e = 7$ mTorr , $p_n = 30$ mTorr.

sition trends and values, regardless of the antenna and bulk and edge plasma densities. Therefore, the above-mentioned considerations related to Fig.4.13 hold true.
Independently of the bulk and edge density values, the Fractional Helix is the least efficient antenna in coupling power. At a bulk density value of 10^{19} m^{-3} and an edge value of 10^{18} m^{-3}, the power deposition curve of a Fractional Helix antenna is close to the power deposition curve of a Single-Loop antenna working with a bulk density value of 10^{18} m^{-3} and an edge density value of 10^{17} m^{-3}.

Chapter 5

Conclusions

We have used ADAMANT to analyze the power deposited by an RF antenna into a non-uniform Helicon plasma source with both radial and radial-axial density profiles. We have considered the effect of different bulk and edge plasma densities as well as different plasma discharge parameters (e.g., electron temperature, neutral pressure) on the power deposition, in terms of the real part of the impedance. Three different antenna topologies have been considered: (i) Single-Loop; (ii) Nagoya Type-III; (iii) Fractional Helix.
In order to correctly describe the electromagnetic problem while keeping the simulation time at bay, we have performed a sensibility analysis to identify the number of basis functions to represent the current distribution on the antenna surface, and the electric flux density in the plasma volume. This number is a trade-off solution considering the numerical accuracy of the results, the computational times and the numerical instability. The results show that:

- The density profiles affect the magnitude of power deposited into the plasma. The Single-Loop antenna has a different trend of power deposition as a function of the magneto-static field compared to the Nagoya Type-III and Fractional Helix antennas. For given bulk and edge density values, electron temperature and neutral pressure, the antennas couple power more efficiently with $n(10, 1, r)$ and $n(10, 1, r, z)$ density profiles. Regardless of antenna and density profile, the non-uniform density curves are close to the uniform curves corresponding to the highest density values achieved in non-uniform configurations;

- For a given bulk density value, each antenna deposits more power the greater the difference between bulk and edge density values. This effect is enhanced for $n(2, 1, r)$ profiles. Regardless of the edge density value nad for magneto-static field values below < 200 G, the Single-Loop and the Nagoya Type-III antennas couple power more efficiently with a high bulk density value (i.e., $n_{bulk} = 10^{19}\ m^{-3}$). The trend is reversed for magneto-static field values $B_0 > 200$ G. In addition, the peak of the power deposition shifts from low magneto-static field values ($B_0 < 100$ G) to higher magneto-static field values ($B_0 > 200$ G), as the bulk density value increases from $n_{bulk} = 10^{18}\ m^{-3}$ to $n_{bulk} = 10^{19}\ m^{-3}$;

- The electron temperature has no relevant effect on the trends and magnitude of

the real part of the impedance. Regardless of the plasma density profile and bulk and edge density values, the Single-Loop is the most efficient antenna in coupling power into a 3 eV plasma. At low bulk-edge density values (i.e., $n_{bulk} = 10^{18}\ m^{-3}$, $n_{edge} = 5 \times 10^{17}\ m^{-3}$) the power deposition curves of the Nagoya Type-III and the Fractional Helix antennas are well separated for magneto-static field values below < 200 G, while are overlapped for $B_0 > 300$ G. At higher bulk-edge density values (i.e., $n_{bulk} = 10^{19}\ m^{-3}$, $n_{edge} = 5 \times 10^{18}\ m^{-3}$) and for $B_0 < 300$, the Nagoya Type-III and the Fractional Helix antennas deposit more power with $T_e = 3$ eV; the opposite can be found for $B_0 > 300$ G;

- The neutral pressure has no relevant effect on the trends and magnitude of the real part of the impedance. Regardless of the plasma density profile and bulk and edge density values, the Single-Loop is the most efficient antenna in coupling power into a 15 mTorr plasma. At low bulk-edge density values (i.e., $n_{bulk} = 10^{18}\ m^{-3}$, $n_{edge} = 5 \times 10^{17}\ m^{-3}$) the power deposition curves of the Nagoya Type-III and the Fractional Helix antennas are well separated for magneto-static field values below < 200 G, while are overlapped for $B_0 > 300$ G. At higher bulk-edge density values (i.e., $n_{bulk} = 10^{19}\ m^{-3}$, $n_{edge} = 5 \times 10^{18}\ m^{-3}$) no clear trend can be evidenced, the power deposition being function of the antenna, magneto-static field and neutral pressure values;

- The Single-Loop is the most efficient antenna in power deposition at low bulk-edge density values (i.e., $n_{bulk} = 10^{18}\ m^{-3}$, $n_{edge} = 10^{17}\ m^{-3}$) for all magneto-static field values explored. This holds true for higher bulk-edge density values (i.e., $n_{bulk} = 10^{19}\ m^{-3}$, $n_{edge} = 10^{18}\ m^{-3}$) and low magneto-statico field values (i.e., $B_0 < 300$ G); for higher magneto-static field values $B_0 > 300$ G, the Nagoya Type-III antenna is the most efficient at coupling power. Regardless of the density profile and bulk-edge pair, the Fractional Helix always reaches low values of power deposition compared to other antennas.

Bibliography

[1] S. M. Tysk, C. M. Denning, J. E. Scharer, K. Akhtar, "Optical, Wave Measurements, and Modeling of Helicon Plasmas for a wide range of Magnetic Fields," *Physics of Plasmas*, vol. 11, no. 3, 2004.

[2] C. M. Denning, M. Wiebold, J. E. Scharer, ""Observations of Neutral Depletion and Plasma Acceleration in a flowing High-Power Argon Helicon Plasma," *Physics of Plasmas*, 2008.

[3] T. H. Stix, *The Theory of Plasma Waves*, New York, 1962.

[4] ——, *Waves in Plasmas*, AIP, New York, 1992.

[5] F. Tong-Zhen, W. Long, J. Di-Ming, Z. Hou-Xian, "Helicon Discharge using a Nagoya Type III Antenna," *Chinese Physics Letters*, vol. 18, no. 8, p. 1098, 2001.

[6] R. Gallet, J. M. Richardson, B. Wieder, G. D. Ward, "Microwave Whistler mode Propagation in a Dense Laboratory Plasma," *Physical Review Letters*, vol. 4, 1960.

[7] H. Blevin, P. Thonemann, Tech. Rep. CLM-R66, 1966.

[8] J. Lehane, P. Thonemann, "An Experimental Study of Helicon Wave Propagation in a Gaseous Plasma," *Proceedings of the Physical Society*, 1965.

[9] R. Boswell, "Modulated RF produced Argon Magneto-plasma," School of Physical Sciences, Finders University, Australia, Tech. Rep. PR 68/8, 1968.

[10] T. Watari, T. Hatori, R. Kumasawa, S. Hidekuma et al., "Radio-Frequency Plugging of a High Density Plasma," *Physics of Fluids*, 1978.

[11] R. Boswell, R. Porteous, A. Prytz, A. Bouchoule, "Some Features of RF excited Fully Ionized Low Pressure Argon Plasma," *Physical Letters A*, 1982.

[12] F. F. Chen, D. Arnush, "Generalized theory of Helicon Waves. i. Normal Modes," *Physical Plasmas*, vol. 4, no. 9, 1997.

[13] A. W. Trivelpiece, R. W. Gould, *Journal of Applied Physics*, 1959.

[14] D. Arnush, F. F. Chen, "Generalized theory of Helicon Waves. ii. Excitation and Absorption," *Physical Plasmas*, vol. 5, no. 5, May 1998.

[15] F. F. Chen, *Experiments on Helicon Plasma Source.*

[16] F. F. Chen, "Plasma Ionization by Helicon Waves," *Plasma Physics and Controlled Fusion*, vol. 33, no. 4, p. 339, 1991.

[17] F. F. Chen, D. D. Blackwell, *Upper Limit to Landau Damping in Helicon Discharges*, 1998.

[18] K. P. Shamrai, V. P. Pavlenko, V. B. Taranov, *Plasma Physics Controlled Fusion*, no. 39, p. 505, 1997.

[19] Y. Mouzouris, J. E. Scharer, "Modeling of Profile Effects for Inductive Helicon Plasma Source," *IEEE Transactions on Plasma Science*, vol. 24, no. 1, Feb. 1996.

[20] L. Berry, J. Whitson, 1996.

[21] D. Arnush, "Role of Trivelpiece-Gould Waves in Antenna Helicon Wave Coupling," *Physical Plasmas*, vol. 7, pp. 3042–3050, 2000.

[22] Y. Mouzouris, J. E. Scharer, "Two-Dimensional (r,z) Plasma Wave Absorption and Poynting Flux Simulations for Helicon Sources," *IEEE Transactions on Plasma Science*, vol. 27, no. 1, Feb. 1999.

[23] ——, "Modeling of Profile Effects for Inductive Helicon Plasma Source," *IEEE Transactions on Plasma Science*, vol. 24, no. 152, Feb. 1996.

[24] D. Melazzi, D. Curreli, M. Manente, J. Carlsson, D. Pavarin, "SPIREs: A Finite-Difference Frequency-Domain Electromagnetic Solver for Inhomogeneous Plasma Cylinders," *Computer Physics Communications*, vol. 183, 2012.

[25] D. Melazzi, V. Lancellotti, "ADAMANT: A Surface and Volume Integral-Equation Solver for the Analysis and Design of Helicon Plasma Sources," *Computer Physics Communications*, Feb. 2014.

[26] D. Pavarin, F. Ferri, M. Manente et al., "Design of 50W Helicon Plasma Thruster," Ann Arbor, Michigan, USA, Tech. Rep. IEPC-2009.

[27] F. Diaz, "The VASIMR Rocket," *Scientific American*, vol. 283, no. 5, 2000.

[28] D. Pavarin, F. Ferri, M. Manente et al., "Helicon Plasma Hydrazine Combined Micro," Milan, Italy, 2009, XX AIDAA Congress.

[29] D. Pavarin et al., "Helicon Plasma Hydrazine Combined Micro Project Overview and Development Status," in *Proceedings of Space Propulsion Conference*, San Sebastian, Spain, 2010.

[30] J. Gilland, G. Piefer, "*40th AIAA/ASME/SAE/ASEE Joint Propulsion Conference and Exhibit*," 2004.

[31] D. Melazzi, V. Lancellotti, M. Manente, D. Pavarin, "Antenna Design and Optimization for Helicon Plasma Thruster with Coupled Surface and Volume Integral Equations," Turin, Italy, 2013, ICEAA Conference.

[32] S. Rao, D. Wilton, A. Glisson, "Electromagnetic Scattering by Surfaces of Arbitrary Shape," *IEEE Transactions on Antennas and Propagation*, vol. 30, pp. 409–418, 1982.

[33] D. H. Schaubert, D. R. Wilton, A. Glisson, "A Tetrahedral Modeling Method for Electromagnetic Scattering by Arbitrarily Shaped Inhomogeneous Dielectric Bodies," *IEEE Transactions on Antennas and Propagation*, vol. 32, pp. 77–85, 1984.

[34] C. Geuzain, J. Remacle, "GMSH: a Three-Dimensional Finite Element Mesh Generator with Built-in Pre- and Post-Processing Facilities."

[35] D. Melazzi, V. Lancellotti, "A Comparative Study of Radio-Frequency Antennas for Helicon Plasma Sources," 2014, *submitted to Plasma Source Science and Technology.*

[36] D. Melazzi, D. Pavarin, M. Manente, A. Cardinali, "Helicon Source for Plasma Thruster: Power Deposition Parametric Study," 2014, *submitted to Plasma Source Science and Technology.*

[37] F. F. Chen, "Helicon Waves at Low Magnetic Fields," no. PPG-1270, Oct. 1989.